

Hadron collisions at ultrahigh energies: black disk or resonant disk modes?

V.V. Anisovich⁺, V.A. Nikonov^{+◇} and J. Nyiri^{*}

March 8, 2019

⁺*National Research Centre "Kurchatov Institute", Petersburg Nuclear Physics Institute, Gatchina, 188300, Russia*

[◇]*Helmholtz-Institut für Strahlen- und Kernphysik, Universität Bonn, Germany*

^{*}*Institute for Particle and Nuclear Physics, Wigner RCP, Budapest 1121, Hungary*

Abstract

The analysis of current ultrahigh energy data for hadronic total cross sections and diffractive scattering cross sections points to a steady growth of the optical density with energy for elastic scattering amplitudes in the impact parameter space, b . At LHC energy the profile function of the pp -scattering amplitude, $T(b)$, reaches the black disk limit at small b . Two scenarios are possible at larger energies, $\sqrt{s} \gtrsim 100$ TeV. First, the profile function gets frozen in the black disk limit, $T(b) \simeq 1$ while the radius of the black disk $R_{black\ disk}$ is increasing with \sqrt{s} , providing $\sigma_{tot} \sim \ln^2 s$, $\sigma_{el} \sim \ln^2 s$, $\sigma_{inel} \sim \ln^2 s$. In another scenario the profile function continues to grow at $\sqrt{s} \gtrsim 100$ TeV approaching the maximal value, $T(b) \simeq 2$, that means the resonant disk mode. We discuss features of the resonant disk mode when the disk radius, $R_{resonant\ disk}$, increases providing the growth of the total and elastic cross sections $\sigma_{tot} \sim \ln^2 s$, $\sigma_{el} \sim \ln^2 s$, but a more slow increase of inelastic cross section, $\sigma_{inel} \sim \ln s$.

PACS: 13.85.Lg 13.75.Cs 14.20.Dh

1 Introduction

The data [1, 2] definitely confirm the previous observations [3], namely, that the total cross sections increase steadily with energy ($\sigma_{tot} \sim \ln^n s$ as $1 \lesssim n \lesssim 2$); the steady growth is observed for σ_{el} and σ_{inel} , while the ratio ReA_{el}/ImA_{el} is small and probably decreases slowly.

Already the first indications of the cross sections growth [4] gave start to corresponding models with the supercritical pomeron [5, 6]. The concept of the power growth of cross sections ($\sigma_{tot} \sim s^\Delta$ with $\Delta \simeq 0.08$) became widely accepted in the 1980s [7, 8] and is discussed till now [9] (let us note that exceeding of the Froissart bound [10] does not violate necessarily the general constraints [11]).

It was shown in [12, 13, 14] that the power-type growth of scattering amplitudes is dumped to $\ln^2 s$ -type within the s -channel unitarization. The black disk picture with the $\ln^2 s$ -growth of the σ_{tot} and σ_{el} at ultrahigh energies was suggested in the Dakhno-Nikonov model [15]. The model can be considered as a realization of the Good-Walker eikonal approach [16] for a continuous set of channels. Presently, the black disk mode for hadron collisions at ultrahigh energies is discussed extensively, see, for example, [17, 18, 19, 20, 21, 22].

The black disk mode is usually discussed in terms of the optical density for elastic scattering amplitude. For the asymptotic regime such a presentation was carried out in [23, 24]: the cross sections $\sigma_{tot}(pp)$, $\sigma_{el}(pp)$, $\sigma_{inel}(pp)$ demonstrate a maximal growth, $\sim \ln^2 s$, while diffractive dissociation cross sections $\sigma_D(pp)$, $\sigma_{DD}(pp)$ give a slower growth, $\sim \ln s$.

For the calculation of screening corrections in inelastic diffractive processes at ultrahigh energies [25] the K -matrix technique is more preferable. The K -matrix function $-iK(b)$ in the preLHC region increases with energy being mainly concentrated at $b < 1$ fm. The black disk regime for the K -matrix function means its "freezing", $-iK(b) \rightarrow 1$, in the disk area. If the growth of the $-iK(b)$ continues with increasing energy, the interaction area turns into a resonant disk. In this case asymptotically $\sigma_{tot}(pp) \sim \ln^2 s$, $\sigma_{el}(pp) \sim \ln^2 s$ with $[\sigma_{el}(pp)/\sigma_{tot}(pp)]_{s \rightarrow \infty} \rightarrow 1$; the resonant disk area is surrounded by a black border band that provides $\sigma_{inel}(pp) \sim \ln s$, $\sigma_D(pp) \sim \ln s$, $\sigma_{DD}(pp) \sim \ln s$.

At present paper we perform comparative analysis of predictions for ultrahigh energy diffractive processes under these two scenarios. For resonant disk mode we consider a power growth with energy $-iK(b) \sim s^\Delta$ but variants with a more slow growth, $-iK(b) \sim \ln^n s$, are possible as well.

2 Scattering amplitude in the impact parameter space and the K -matrix representation for ultrahigh energy

In the impact parameter space the profile function $T(b)$ is determined at high energies as:

$$\begin{aligned} \sigma_{tot} &= 2 \int d^2b T(b), \\ 4\pi \frac{d\sigma_{el}}{d\mathbf{q}_\perp^2} &= |A_{el}(\mathbf{q}_\perp^2)|^2, \quad A_{el}(\mathbf{q}_\perp^2) = i \int d^2b e^{i\mathbf{b}\mathbf{q}_\perp} T(b), \\ T(b) &= 1 - \eta(b) e^{2i\delta(b)} = 1 - e^{-\frac{1}{2}\chi(b)} = \frac{-2iK(b)}{1 - iK(b)}, \end{aligned} \tag{1}$$

here $A_{el}(\mathbf{q}_\perp^2)$ is the elastic scattering amplitude. The profile function can be presented either in the standard form using the inelasticity parameter $\eta(b)$ and the phase shift $\delta(b)$ or in terms of the optical density $\chi(b)$ and the K -matrix function $K(b)$. The K -matrix approach is based on the separation of the elastic rescatterings in the intermediate states: the function $K(b)$ includes only the multiparticle states thus being complex valued. The small value of the ReA_{el}/ImA_{el} tells that $K(b)$ is dominantly imaginary.

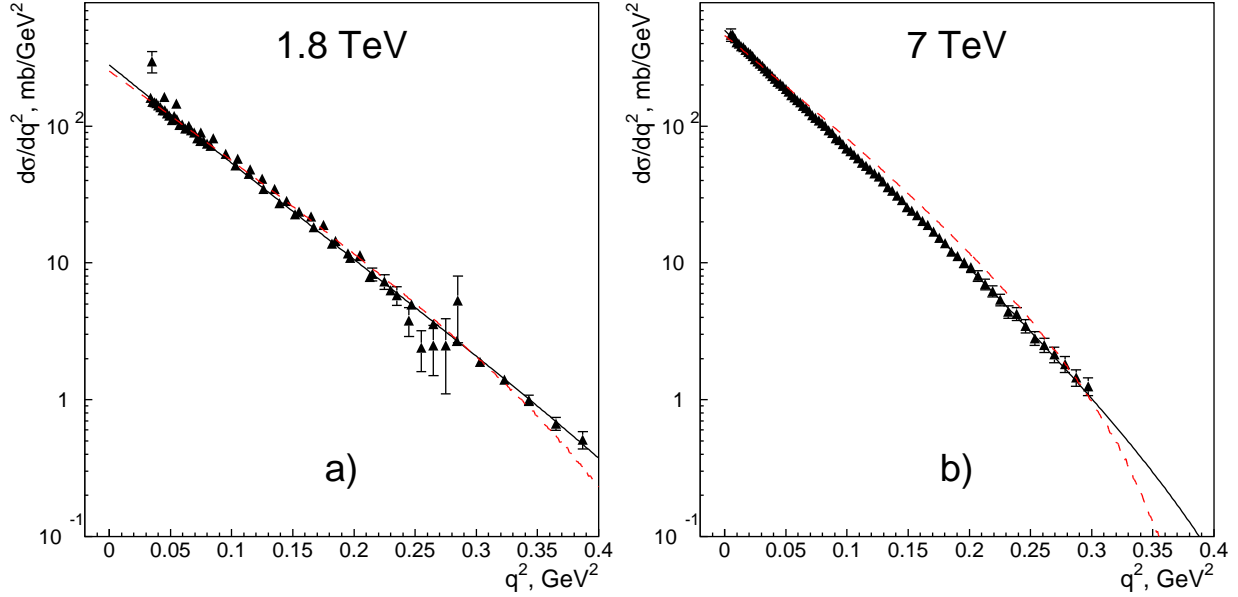


Figure 1: a,b) Differential cross sections $d\sigma_{el}/dq_{\perp}^2$ at $\sqrt{s} = 1.8, 7.0$ TeV and their description within the black disk mode (red dashed lines) and the resonant disk mode (solid lines).

2.0.1 Black disk limit in terms of the Dakhno-Nikonov model

The Dakhno-Nikonov model [15] demonstrates us a representative example of application of the optical density technique for the consideration of pp^{\pm} collisions at ultrahigh energies when $\ln s \gg 1$. In the model the black disk is formed by the low density pomeron cloud and rescatterings are described within the eikonal approach. The scattering amplitude $AB \rightarrow AB$ reads:

$$A_{AB \rightarrow AB}(\mathbf{q}^2) = i \int d^2b e^{i\mathbf{q}\mathbf{b}} \int dr' \varphi_A^2(r') dr'' \varphi_B^2(r'') \left[1 - \exp\left(-\frac{1}{2}\chi_{AB}(r', r'', \mathbf{b})\right) \right], \quad (2)$$

where $dr\varphi_A^2(r)$, $dr\varphi_B^2(r)$ are the quark densities of the colliding hadrons in the impact parameter space. Proton and pion quark densities can be determined using the corresponding form factors. The optical density $\chi_{AB}(r', r'', \mathbf{b})$ depends on parameters of the t -channel interaction.

The behavior of amplitudes at ultrahigh energies is determined by leading complex- j singularities, in the Dakhno-Nikonov model that are leading and next-to-leading pomerons with trajectories $\alpha(\mathbf{q}^2) \simeq 1 + \Delta - \alpha' \mathbf{q}^2$. The fit of refs. [22, 23] gives:

parameters	leading pole	next-to-leading
Δ	0.27	0
$\alpha'_P [(\text{GeV})^{-2}]$	0.13	0.25

(3)

In terms of the K-matrix approach the black disk mode means assumed freezing of the $-iK(b)$ in the interaction area:

$$\begin{aligned} \left[-iK(b) \right]_{\xi \rightarrow \infty} &\rightarrow 1 && \text{at } b < R_0 \xi, \\ \left[-iK(b) \right]_{\xi \rightarrow \infty} &\rightarrow 0 && \text{at } b > R_0 \xi, \end{aligned} \quad (4)$$

$$\xi = \ln \frac{s}{s_R}, \quad s_R \simeq 6.4 \cdot 10^3 \text{ GeV}^2, \text{ with } R_0 \simeq 2\sqrt{\alpha' \Delta} \simeq 0.08 \text{ fm.}$$

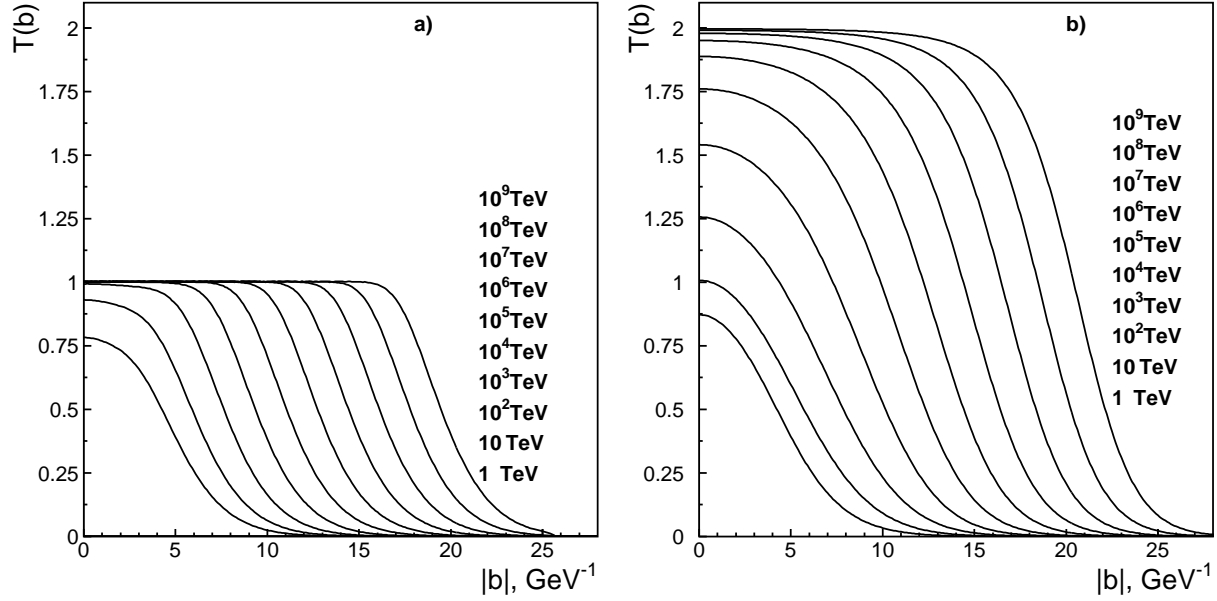


Figure 2: a) Profile functions, $T(b)$, at $\sqrt{s} = 1, 10, 10^2, \dots, 10^9$ TeV for the black disk regime ($T(b) \rightarrow 1$) and b) resonant disk regime ($T(b) \rightarrow 2$).

The growth of the radius of the black disk is slow: small value of R_0 is caused by the large mass of glueballs [26, 27] and the effective mass of gluons [28, 29].

The black disk mode results in

$$\begin{aligned} \sigma_{tot} &\simeq 2\pi(R_0\xi)^2, \\ \sigma_{el} &\simeq \pi(R_0\xi)^2, \quad \sigma_{inel} \simeq \pi(R_0\xi)^2. \end{aligned} \quad (5)$$

For the black disk radius the corrections of the order of $\ln \xi$ exist $R_{black\ disk} \simeq R_0\xi + \varrho \ln \xi$ but they become apparent in the Dakhno-Nikonov model at energies of the order of the Plank mass, $\sqrt{s} \sim 10^{17}$ TeV.

2.0.2 Resonant disk and K-matrix function

From the data it follows that both $T(b)$ and $-iK(b)$ are increasing with energy, being less than unity. If the eikonal mechanism does not quench the growth, both characteristics cross the black disk limit getting $T(b) > 1$, $-iK(b) > 1$. If $-iK(b) \rightarrow \infty$ at $\ln s \rightarrow \infty$, which corresponds to a growth caused by the supercritical pomeron ($\Delta > 0$), the diffractive scattering process gets to the resonant disk mode.

For following the resonant disk switch-on we use the two-pomeron model with parameters providing the description of data at 1.8 TeV and 7 TeV, namely:

$$\begin{aligned} -iK(b) &= \int \frac{d^2q}{(2\pi)^2} \exp(-i\mathbf{q}\mathbf{b}) \sum g^2 s^\Delta e^{-(a+\alpha\xi)\mathbf{q}^2} \\ &= \sum \frac{g^2}{4\pi(a+\alpha'\xi)} \exp\left[\Delta\xi - \frac{\mathbf{b}^2}{4(a+\alpha'\xi)}\right], \quad \xi = \ln \frac{s}{s_0}. \end{aligned} \quad (6)$$

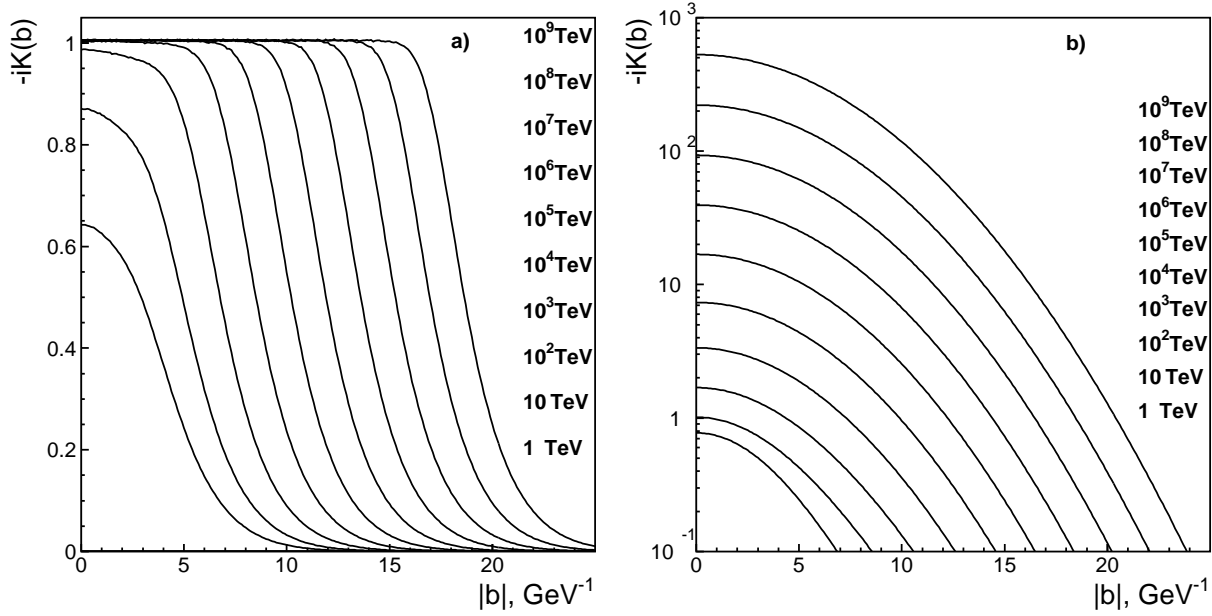


Figure 3: The K-matrix functions, $-iK(b)$, for a) the black disk mode ($[-iK(b)]_{\xi \rightarrow \infty} \rightarrow 1$ at $b < R_0\xi$) and b) the resonant disk mode ($[-iK(b)]_{\xi \rightarrow \infty} \rightarrow \infty$ at $b < R_0\xi$).

The following parameters are found for the leading and the next-to-leading pomerons :

parameters	leading pole	next-to-leading
Δ	0.20	0
α'_P [GeV $^{-2}$]	0.18	0.14
a [GeV $^{-2}$]	6.67	2.22
g^2 [mb]	1.74	28.6
s_0 [GeV 2]	1	1

(7)

The description of the differential cross sections $d\sigma_{el}/d\mathbf{q}_\perp^2$ at $\sqrt{s} = 1.8, 7.0$ TeV in resonant disk mode is demonstrated in Fig. 1. Resonant interaction regime occurs at $b < 2\sqrt{\alpha'\Delta}\xi = R_0\xi$, in this region $T(b) \rightarrow 2$. In terms of the inelasticity parameter and the phase shift it corresponds to $\eta \rightarrow 1$ and $\delta \rightarrow \pi/2$. Cross sections at $\xi \rightarrow \infty$ obey $\sigma_{tot} \simeq 4\pi R_0^2\xi^2$, $\sigma_{el}/\sigma_{tot} \rightarrow 1$ and $\sigma_{inel} \simeq 2\pi R_0\xi$.

2.0.3 Comparative survey of the resonant disk and black disk modes

At the energy $\sqrt{s} \sim 10$ TeV the black cloud fills out the proper hadron domain, the region ≤ 1 fm, and that happens in both modes. It is demonstrated in Figs. 2,3: the profile functions $T(b)$ coincide practically in both modes as well as the K-functions $-iK(b)$. Correspondingly, the differential cross sections in τ -representation differ a little, mainly at $\tau \sim 10$, Fig. 4. The energy behavior of σ_{tot} , σ_{el} and σ_{inel} coincide also at $\sqrt{s} \sim 1 - 100$ TeV in both modes, Fig. 5.

Differences appear at $\sqrt{s} \sim 1000$ TeV: $T(b) \simeq 1.5$ at $b \lesssim 0.5$ fm and the black zone has shifted to $b \simeq 1.0 - 1.5$ fm, Fig. 3b. With further energy increase the radius of the black band increases as $2\sqrt{\Delta\alpha'}\xi \equiv R_{rd}\xi$. The rate of growth in both modes is determined by the leading singularity and the fit of the data in the region $\sqrt{s} \sim 1 - 10$ TeV gives approximately the same values of Δ and α' for both cases thus providing $R_0 \simeq R_{rd}$.

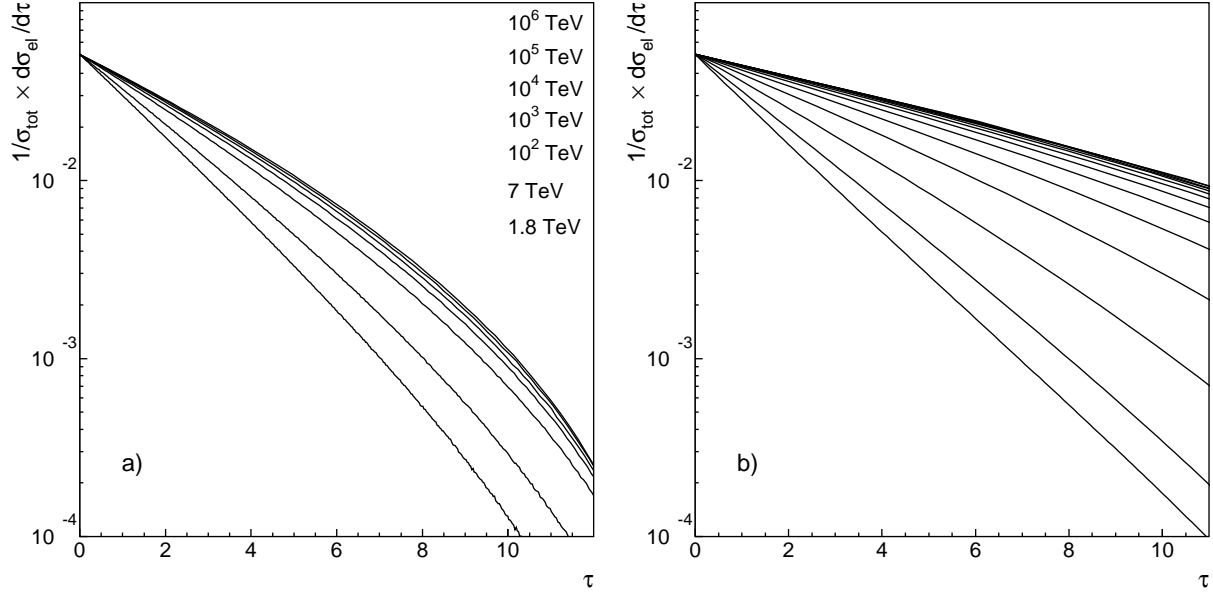


Figure 4: The τ -representation ($\tau = \sigma_{tot} \mathbf{q}^2$) for differential cross section, $\frac{1}{\sigma_{tot}} \frac{d\sigma_{el}}{d\tau}$, for the black disk (a) and resonant disk (b) modes.

2.0.4 Logarithmic growth of the $K(b)$ -function

More slow growth of $-iK(b)$ with energy than power, the logarithmic one, reads:

$$\begin{aligned} -iK(b) &= \int \frac{d^2q}{(2\pi)^2} \exp(-i\mathbf{q}\mathbf{b}) g^2 \xi^N \exp[-\alpha' \xi^n \mathbf{q}^2] \\ &= \frac{g^2}{4\pi\alpha'} \xi^{N-n} \exp\left[-\frac{\mathbf{b}^2}{4\alpha' \xi^n}\right], \quad \text{with } N > 0, n > 0. \end{aligned} \quad (8)$$

For the scattering amplitude eq. (8) gives:

$$\begin{aligned} A_{el}(\mathbf{q}^2) &= 2 \int d^2b e^{i\mathbf{b}\mathbf{q}} \frac{K(b)}{1 - iK(b)} \\ &= 2i\xi^n \int d^2\beta e^{i\beta\boldsymbol{\kappa}} \frac{\frac{g^2}{4\pi\alpha'} \xi^{N-n} \exp[-\frac{\beta^2}{4\alpha'}]}{1 + \frac{g^2}{4\pi\alpha'} \xi^{N-n} \exp[-\frac{\beta^2}{4\alpha'}]}, \quad \beta = \frac{\mathbf{b}}{\xi^{n/2}}, \quad \boldsymbol{\kappa} = \mathbf{q}\xi^{n/2}. \end{aligned} \quad (9)$$

At $N - n > 0$ we have resonant disk picture. The disk radius squared increases with energy as $R_{disk}^2 \simeq 4\alpha'(N - n)\xi^2 \ln \xi + g^2 \xi^2$ but the terms of the $\ln \ln s$ -type are essential at \sqrt{s} of the order of the Plank mass.

3 Conclusion

The interaction of soft gluons determines the physics of hadrons. The effective gluons are massive and their mass is of the order of 1 GeV that is seen directly in radiative decays of heavy quarkonia [28, 29], $\psi \rightarrow \gamma + \text{hadrons}$ and $\Upsilon \rightarrow \gamma + \text{hadrons}$. The effective gluon mass is determinative both for low energy physics, making possible to introduce the notion

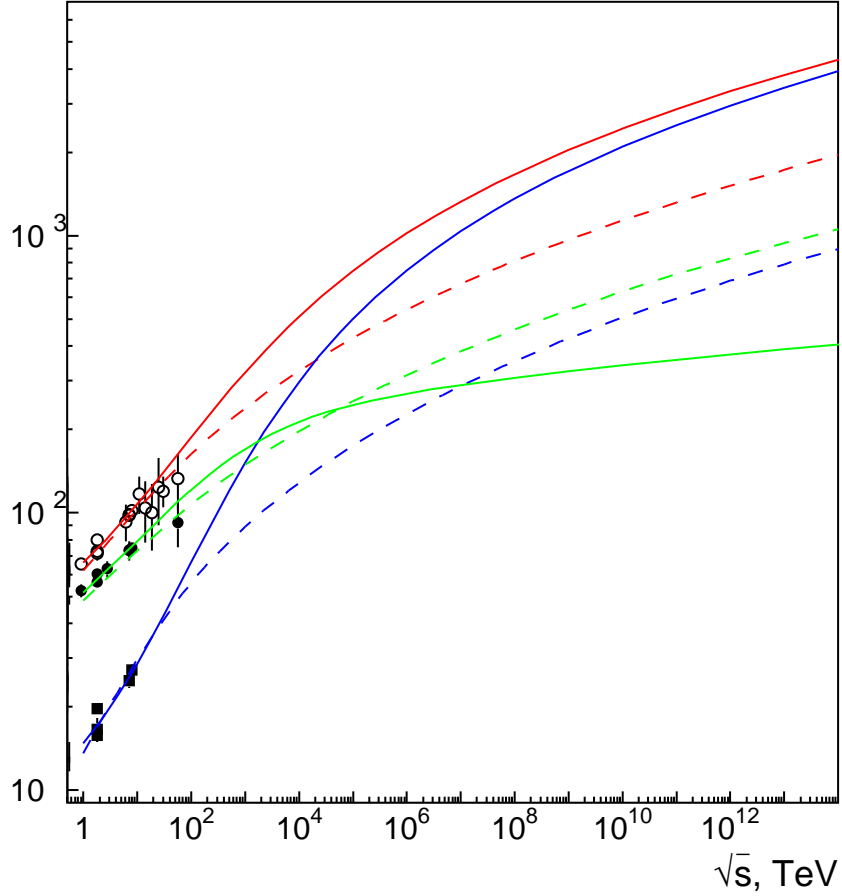


Figure 5: Total, elastic and inelastic cross sections for resonant disk (solid lines) and black disk (dashed lines) modes: red σ_{tot} , blue σ_{el} , green σ_{inel} .

of the constituent quark, and for high energy physics, dictating the rate of the growth of the interaction radius. High energy physics is the physics of large logarithms, $\ln s/s_0 \gg 1$, and the value $\sqrt{s_0} \sim m_{effective\ gluon}$ corresponds to a start of the asymptotic regime at $\sqrt{s} \sim 1$ TeV. However, the initial increments of the measured characteristics such as σ_{tot} , σ_{el} and σ_{inel} are visually similar, and therefore their behavior in this region does not discriminate different versions. A real discrimination of modes can appear when cross section data are discussed at much larger energies, $\sqrt{s} \sim 10^3 - 10^4$ TeV.

References

- [1] G. Latino for the TOTEM collaboration, *Summary of Physics Results from the TOTEM Experiment*, arXiv:1302.2098(2013) [hep-ph].
- [2] Pierre Auger Collaboration (P. Abreu *et al.*), Phys. Rev. Lett. **109**, 062002 (2012).
- [3] UA4 Collaboration, Phys. Lett. **B147**, 385 (1984);
 UA4/2 Collaboration, Phys. Lett. **B316**, 448 (1993);
 UA1 Collaboration, Phys. Lett. **B128**, 336 (1982);

- E710 Collaboration, Phys. Lett. **B247**, 127 (1990);
CDF Collaboration, Phys. Rev. **D50**, 5518 (1994).
- [4] Y.P. Gorin *et al.* Yad. Phys. **14**, 998 (1971).
 - [5] A. Capella and J. Kaplan, Phys. Lett. **B52**, 448 (1974).
 - [6] P.E. Volkovitsky, M.A. Lapidus, V.I. Lisin, K.A. Ter-Martirosyan, Yad. Phys. **24**, 1237 (1976).
 - [7] A. Donnachie and P.V. Landshoff, Nucl. Phys. **B231**, 189 (1984).
 - [8] A.B. Kaidalov and K.A. Ter-Martirosyan, Sov. J. Nucl. Phys. **39**, 979 (1984).
 - [9] A. Donnachie and P.V. Landshoff, arXiv:11122485, (2011) [hep-ph].
 - [10] M. Froissart, Phys. Rev. **123**, 1053 (1961).
 - [11] Y.I. Azimov, Phys. Rev. **D84**, 056012 (2011); arXiv:1208.4304(2012) [hep-ph].
 - [12] T.K. Gaisser and T. Stanev, Phys. Lett., **B219**, 375, 1989.
 - [13] M. Block, F. Halzen and B. Margolis, Phys. Lett., **B252**, 481, 1990.
 - [14] R.S. Fletcher, Phys. Rev. **D46**, 187, 1992.
 - [15] L.G. Dakhno and V.A. Nikonov, Eur. Phys. J. **A8**, 209 (1999).
 - [16] M.L. Good, W.D. Walker, Phys. Rev. **120**, 1857 (1960).
 - [17] F. Halzen, K. Igi, M. Ishida and C.S. Kim, Phys. Rev. **D85**, 074020 (2012); arXiv:1110.1479V2(2012) [hep-ph].
 - [18] V. Uzhinsky and A. Galoyan, arXiv:1111.4984v5(2012) [hep-ph].
 - [19] M.G. Ryskin, A.D. Martin and V.A. Khoze, Eur. Phys. J. **C72**, 1937(2012); arXiv:1201.6298v2(2012) [hep-ph].
 - [20] I.M. Dremin, V.A. Nechitailo, Phys. Rev. **D85**, 074009 (2012); arXiv:1202.2016 (2012) [hep-ph].
 - [21] M.M. Block and F. Halzen, Phys. Rev. **D86**, 0501504 (2013); arXiv:1208.4086v1 (2012) [hep-ph].
 - [22] V.V. Anisovich, K.V. Nikonov, and V.A. Nikonov, Phys. Rev. **D88**, 014039 (2013); [arXiv:1306.1735 (hep-ph)].
 - [23] V.V. Anisovich, V.A. Nikonov, and J. Nyiri, Phys. Rev. **D88**, 014039 (2013); [arXiv:1310.2839 (hep-ph)].
 - [24] V.V. Anisovich, K.V. Nikonov, V.A. Nikonov and J. Nyiri, Int. J. Mod. Phys. **A29**, 1450096 (2014); arXiv:1404.1904 (hep-ph).

- [25] V.V. Anisovich, M.A. Matveev, and V.A. Nikonov, *Hadron diffractive production at ultra-high energies*, arXiv:1407.4588 (hep-ph).
- [26] V.V. Anisovich, AIP Conf. Proc. **619**, 197 (2002), **717**, 441 (2004); Phys.Usp. **47**, 45 (2004), [UFN **47**, 49 (2004)].
- [27] V.V. Anisovich, M.A. Matveev, J. Nyiri, A.V. Sarantsev, Int. J. Mod. Phys. **A20**, 6327 (2005).
- [28] G. Parisi and R. Petronzio, Phys. Lett. **94**, 51 (1980).
- [29] M. Consoli and J.H. Field, Phys. Rev. **D49**, 1293 (1994).